EurJIC
European Journal of Inorganic Chemistry

Research Article
doi.org/10.1002/ejic.202400162

Chemistry Europe
European Chemical Societies Publishing

www.eurjic.org

Magnetic Single-Ion Anisotropy and Curie-Weiss Behaviour of $Mg_3V_4(PO_4)_6$

Björn Schwarz*[a] and Qiang Fu[a]

Direct current (DC) magnetometry data obtained for polycrystalline $Mg_3V_4(PO_4)_6$ were fitted by various magnetic models based on angular momentum basis states. As a result, single-ion anisotropy of the magnetic V^{3+} ions could be identified to decisively determine the magnetic properties of $Mg_3V_4(PO_4)_6$ and not antiferromagnetic exchange interaction between V ions as supposed in literature. It could be demonstrated analytically, by utilization of the Van Vleck equation, that also single-ion anisotropy can lead to a linear and origin shifted inverse susceptibility curve in the high temperature region. The Weiss constant obtained from a Curie-Weiss fit to such a susceptibility curve might falsely be ascribed to antiferromagnetic exchange interactions if additional low temperature magnetic properties are not considered for verification.

1. Introduction

The investigation of the reaction mechanism of a $Mg_3V_4(PO_4)_6$/carbon composite as negative electrode for monovalent ion-batteries has recently been published with major contribution from the authors of this work.[1] The guest-ion dependent electrochemical reaction mechanisms upon Li-, Na-, and K-ion insertion were investigated, inter alia, by operando synchrotron X-ray diffraction (SXRD) and absorption spectroscopy (SXAS). Results from DC magnetometry measurements of the pristine polycrystalline $Mg_3V_4(PO_4)_6$ sample were also presented with the focus on the V ions' oxidation state that is most relevant in this context. From a Curie-Weiss[2,3] fit, an effective paramagnetic moment $\mu_{eff} = 2.55(1)\ \mu_B$ per V ion was extracted that is a little bit smaller than the spin-only moment of a V^{3+} in octahedral crystal field ($2.83\ \mu_B$), and a Weiss constant $\theta_{CW} = -51.8(3)$ K has been determined (see Eq. (1)) without any further indications for the occurrence of a Néel phase transition to an antiferromagnetically (AF) ordered state down to 5 K.[1] These values were in agreement with those published previously by Porter et al.[4] who interpreted the negative value of the Weiss constant θ_{CW} as indicative for AF interactions between V^{3+} ions. They assumed that the lack of a Néel transition above 5 K could either be due to weak coupling between isolated dimers or due to geometric frustration. However, our results that took also the low temperature and high field magnetic behaviour into account, suggested that the decisive interaction responsible for the magnetic properties of $Mg_3V_4(PO_4)_6$ should rather be ascribed to single-ion anisotropy than to AF exchange interaction.[1] This work was inspired by the question whether single-ion anisotropy can alternatively cause a Curie-Weiss behaviour with a negative Weiss constant and, if so, how these two interactions can be discriminated from each other?

It is a kind of standard routine, that can be found in a vast number of publications, that the Weiss constant θ_{CW} extracted from a Curie-Weiss fit according to:

$$\chi^{-1} = C_{CW}^{-1} \cdot (T - \theta_{CW}) \quad (1)$$

to the linear, paramagnetic part of the high temperature inverse susceptibility χ^{-1} vs. temperature T plots, is attributed either to ferromagnetic ($\theta_{CW} > 0$) or to AF ($\theta_{CW} < 0$) mean field interactions. This attribution might be legit in cases where a corresponding phase transition to an ordered state at low temperature can be verified but becomes doubtful if this is not the case. Specific aim of this work is on the one side to comprehensively show that single-ion anisotropy determines the magnetic behaviour of $Mg_3V_4(PO_4)_6$ and not AF exchange coupling. This will be done by the refinement of various quantum mechanical (QM) magnetic models to the susceptibility vs. temperature as well as to the low temperature magnetization vs. field DC magnetometry data sets. The Hilbert space for the "magnetic system" will be constructed from the angular momentum basis states that are treated within a phenomenological Hamiltonian approach.[5] On the other side, it will be demonstrated that also single-ion anisotropy leads to a Curie-Weiss behaviour identical to that caused by AF interactions under certain conditions. This will be done by explicitly derive expressions for the magnetic susceptibility of various magnetic models from the Van Vleck equation (see Eq. (2)).

Boudin et al.[6] have first described the structure of the quaternary V^{3+}-containing phosphate compound, $Zn_3V_4(PO_4)_6$, by single crystal XRD. It crystallizes in the triclinic space group $P\bar{1}$ in the $Fe_7(PO_4)_6$ structure type. Porter et al.[4] synthesized a

[a] Dr. B. Schwarz, Dr. Q. Fu
Karlsruhe Institute of Technology (KIT)
Institute for Applied Materials (IAM)
Herrmann-von-Helmholtz-Platz 1
76344 Eggenstein-Leopoldshafen, Germany
E-mail: bjoern.schwarz@kit.edu

Supporting information for this article is available on the WWW under https://doi.org/10.1002/ejic.202400162

Research Article
doi.org/10.1002/ejic.202400162

series of $A_3V_4(PO_4)_6$ compounds (A = Mg, Mn, Fe, Co or Ni) and investigated the crystalline structures in detail by combined Rietveld refinements to room-temperature SXRD and neutron powder diffraction (NPD) data sets. They found that all these compounds are isostructural to $Zn_3V_4(PO_4)_6$. Table S1 in the Supporting Information (SI) summarizes the crystallographic structural data of $Mg_3V_4(PO_4)_6$ (ICSD data base under code 252571) as published by Porter et al.[4] The magnetic properties were investigated by DC magnetometry. The susceptibility was measured in the range from 2.5 to 400 K. By a Curie-Weiss fit from 200 to 400 K to the linear region of the inverse susceptibility, an effective moment of $\mu_{eff} = 2.60\,\mu_B$ per V ion and a Weiss constant of $\theta_{CW} = -66.6$ K were extracted for $Mg_3V_4(PO_4)_6$.[4] The negative Weiss constant was interpreted by the authors as indicative for AF interactions between V^{3+} ions as already mentioned above. When magnetic ions Mn, Fe, Co or Ni were substituted on the A-sites for Mg, the magnetic coupling between V_2O_{10} dimers was enhanced and a Néel transition to an AF ordered state was found for these compounds below approximately 15 K.

$Mg_3V_4(PO_4)_6$ offers three crystallographically distinct PO_4^{3-} groups and four unique cation positions: Mg(1) sits on an inversion center ($\bar{1}$), Wyckoff position 1*a*, in a distorted octahedron. It is mainly occupied by Mg^{2+} but partially (~25 %) also by V^{3+}. Mg(2) is exclusively occupied by Mg^{2+} and located on Wyckoff position 2*i* with triclinic (1) point symmetry. It is located within a highly distorted five-coordinate polyhedra. V(1) and V(2) are also located on Wyckoff position 2*i* with triclinic (1) point symmetry in distorted oxygen coordination octahedra. These sites are both mainly (~93 %) occupied by V^{3+} and partially by small amounts of Mg^{2+}. Table 1 lists the distances d_i from the central atoms to the coordinating oxygen atoms for the units $Mg(1)O_6$, $V(1)O_6$ and $V(2)O_6$, with V(1) and V(2) mainly occupied by V ions. $\Delta d_i = \left(d_i - \bar{d}\right) \cdot 100$ are the deviations of the individual metal-oxygen distances d_i from the average value $\bar{d} = \sum_{i=1}^{6} d_i/6$ of a certain MO_6 coordination polyhedra. $Mg(1)O_6$ has quasi orthorhombic point symmetry if only these distances are considered. $V(1)O_6$ and $V(2)O_6$ actually exhibit triclinic point symmetry 1, but it is obvious that one V–O distance is exceptional shorter than the others, pointing to the realization of a strong uniaxial distortion in the first place (see green coloured bonds in Figure 1). The Mg(1) and Mg(2) polyhedra are connected through a common corner to form Mg_2O_{10} units, while the V^{3+} cations reside in V_2O_{10} units composed of two edge-sharing octahedra. An inversion center ($\bar{1}$) lays in the middle of a connection line between V(1)-V(1) and V(2)-V(2), respectively.

Table 1. Distances d_i from the central metal atom to the oxygen coordination atoms, and deviations Δd_i (multiplied with 100) of the individual metal-oxygen distances d_i from the average value $\bar{d}$ for the coordination polyhedra $Mg(1)O_6$, $V(1)O_6$ and $V(2)O_6$. Values are based on the structural data of $Mg_3V_4(PO_4)_6$ published by Porter et al.[4] (ICSD database code 252571).

Central	Coord.	d_i (Å)	Δd_i (Å)
$Mg(1)O_6$			
Mg(1)	O(1)	2.182	7.3
Mg(1)	O(1)	2.182	7.3
Mg(1)	O(4)	1.978	−13.1
Mg(1)	O(4)	1.978	−13.1
Mg(1)	O(5)	2.167	5.8
Mg(1)	O(5)	2.167	5.8
$V(1)O_6$			
V(1)	O(1)	2.077	7.3
V(1)	O(2)	1.820	−18.3
V(1)	O(8)	2.040	3.7
V(1)	O(9)	2.015	1.2
V(1)	O(12)	2.023	2.0
V(1)	O(12)	2.041	3.8
$V(2)O_6$			
V(2)	O(3)	1.993	0.2
V(2)	O(6)	2.070	7.9
V(2)	O(7)	2.025	3.4
V(2)	O(7)	2.055	6.4
V(2)	O(10)	1.877	−11.4
V(2)	O(11)	1.926	−6.5

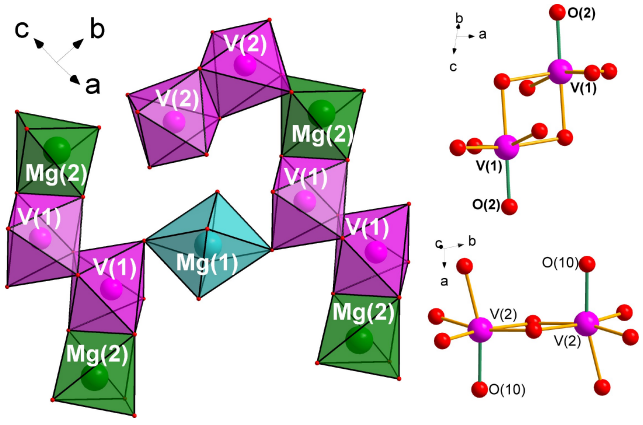

Figure 1. Selected coordination polyhedra and their connections present in the crystal structure of $Mg_3V_4(PO_4)_6$ as published by Porter et al.[4] (ICSD database code 252571). The green coloured connection lines indicate the exceptionally short V(1)-O(2) and V(2)-O(10) distances (see Table 1).

2. Results and Discussion

2.1. Structure and Chemistry

The following results about the structural and chemical characterization of the synthesized $Mg_3V_4(PO_4)_6$ sample have already been published in detail by Fu et al. in Ref. [1] and will only briefly recapitulated here. By synchrotron radiation diffraction, the as-synthesized material was found to be polycrystalline and to exhibit the $Fe_7(PO_4)_6$ structure-type with triclinic space group $P\bar{1}$. All observed reflections can be indexed according to the structural data (ICSD data base code 252571)

Research Article
doi.org/10.1002/ejic.202400162

that have been published already for $Mg_3V_4(PO_4)_6$ by Porter et al.[4] The lattice parameters were refined to $a = 6.325(1)$ Å, $b = 7.903(1)$ Å, $c = 9.286(1)$ Å, $\alpha = 105.287(3)^\circ$, $\beta = 108.567(3)^\circ$, and $\gamma = 101.339(3)^\circ$. By TGA under flowing O_2, the amount of carbon in the as-synthesized material was determined to 4.9 wt%. High resolution transmission electron microscopy (HRTEM) revealed that the sample consists of highly crystalline agglomerated sub micrometer crystallites of the $Mg_3V_4(PO_4)_6$ phase besides smaller aggregated amorphous carbon particles. The edge position of the V K-edge XANES spectrum is almost overlapping with that of the V_2O_3 reference, implying that the V ions are present as V^{3+} in $Mg_3V_4(PO_4)_6$. This is also expected from the charge neutrality condition and the assumption that Mg, P, and O are present as Mg^{2+}, P^{5+} and O^{2-}, respectively.

2.2. Magnetic Properties

The ZFC and FC susceptibility vs. temperature curves measured for $Mg_3V_4(PO_4)_6$ from 2 to 300 K exhibit a slight bifurcation below ~5 K but the full loop magnetization vs. field curve measured at 2 K does not exhibit any detectable hysteresis effect (see Figure S10 and S11 in the SI of Ref. [1]). Both features point to the existence of very small amounts of an additional impurity phase that orders ferri-/ferromagnetically below 5 K. The following data evaluation was therefore restricted to data above 5 K where the magnetic measurements confirmed that there occurs neither a structural nor a magnetic phase transition. Over the broad temperature range from 300 down to 5 K, $Mg_3V_4(PO_4)_6$ remains in the paramagnetic state what is a pre condition to apply the quantum mechanical (QM) phenomenological Hamiltonian magnetic model. Further, the AC susceptibility vs frequency scans performed at 1.8 K (see Figure S1, SI, do not indicate slow relaxing magnetic reversals to be present within the accessible parameter space of the experiment. The phenomenon of (field induced) slow relaxing magnetic reversal can in principle be found for systems where the magnetic moment experiences a strong and purely uniaxial crystal field anisotropy.

2.2.1. Van Vleck Equation and Curie-Weiss Fits

For a measurement of the magnetic susceptibility, the sample is exposed to a uniform magnetic field. In this section, the relation between the Zeeman energy splitting caused by the magnetic field and the magnetic susceptibility is derived analytically by application of a perturbation technique. As outlined in detail in Ref. [7], It is assumed that the wave functions $|\phi_n^{(0)}\rangle$ and their energies $W_n^{(0)}$ of a given system are known at zero magnetic field (the superscripts in brackets represent the order). Other contributions to the Hamiltonian $\hat{H}_0^{(0)}$, as inter electronic interactions, spin-orbit coupling, crystal field effects, magnetic exchange interactions etc. might have already contributed, but not yet the Zeeman term. In the presence of a magnetic field that represents the perturbation and that is chosen to point along the *z*-direction for simplicity, the Hamilton operator is modified to $\hat{H} = \hat{H}_0^{(0)} + B_z\hat{H}_z^{(1)}$ and the energies then change to $E_n = W_n^{(0)} + B_z W_n^{(1)} + B_z^2 W_n^{(2)} + \ldots$, where the $W_n^{(1)}$, $W_n^{(2)}$, etc. are the Zeeman coefficients (that are not energies as $W_n^{(0)}$ is). It should be mentioned at this point that the terms magnetic field H and magnetic induction B that are related in vacuum by $B = \mu_0 H$ (SI), with μ_0 as permeability of vacuum, respectively by $B = H$ (c.g.s) are used synonymously in this work. By knowing the Zeeman coefficients, the magnetic moment components along the field direction $\overline{\mu} = -\partial E_n/\partial B$ for a level can be calculated as $\overline{\mu}_n = -W_n^{(1)} - 2BW_n^{(2)} - \ldots$, and it is possible thereby to calculate the total magnetic moment M as a function of magnetic field B and temperature T by application of the Boltzmann occupation statistics. Finally, the well known Van Vleck formula[7] (Eq. (2)) to calculate the molar magnetic susceptibility from the Zeeman coefficients for small fields and not too low temperatures can be derived (in SI notation):

$$\chi_{mol} = \mu_0 N_A \frac{\sum_n \left[\frac{(-W_n^{(1)})^2}{k_B T} - 2W_n^{(2)}\right] \exp\frac{-W_n^{(0)}}{k_B T}}{\sum_n \exp\frac{-W_n^{(0)}}{k_B T}}. \quad (2)$$

This Van Vleck formula has been used to calculate the molar magnetic susceptibility χ_{mol} for four scenarios that are of special interest for this work: a) for a free effective spin $S = 1$ as a reference, b) for two spins $S_1 = S_2 = 1/2$ that couple AF via an isotropic exchange interaction $J_{iso} = J < 0$, c) for a spin $S = 1$ that experiences uniaxial easy-axis anisotropy parameterized by the zero-field splitting (ZFS) parameter $D' < 0$ and with the magnetic field applied along the easy *z*-axis, and d) for a spin $S = 1$ that experiences uniaxial easy-axis anisotropy parameterized by the zero-field splitting (ZFS) parameter $D' < 0$ but with the magnetic field applied perpendicular to the easy-axis in *x*- or *y*-direction. The detailed derivation of the magnetic susceptibility for all cases is described in the supplementary information in Section S3.1 and Zeeman coefficients as well as the obtained inverse susceptibilities are summarized in Table 2.

Figure 2 shows that χ_{AF}^{-1} (Eq. (4) and Eqs. (S4) to (S9) in SI) and χ_{DX}^{-1} (Eq. (6) and Eqs. (S14) to (S16) in SI) can equally well reproduce the experimentally measured linear χ^{-1} vs. temperature behaviour of $Mg_3V_4(PO_4)_6$ from 150 to 390 K and Table S2 lists the refined parameters. From the Curie constant C_{AF}, an effective moment of $\mu_{eff} = 2.663(2)\ \mu_B$ per V ion has been determined that is only slightly smaller than the spin-only moment $\mu_{so} = \sqrt{8}\,\mu_B \approx 2.83\,\mu_B$ for a spin $S = 1$ pointing to a comparably small contribution from orbital momentum. θ_{AF} that corresponds to the Weiss constant θ_{CW} from the Curie-Weiss law has been refined to −64.8(5) K. At this point it should be mentioned that these values slightly differ from those as published in Ref. [1] that were also mentioned in the introduction since in this work a more elaborate correction of the raw data for diamagnetic contributions has been performed (see Section S4.3). Porter el al.[4] extracted an effective moment of 2.60 μ_B per V ion and a Weiss constant of $\theta_{CW} = -66.6$ K, what is in good agreement with the values determined in this work.

Research Article
doi.org/10.1002/ejic.202400162

Table 2. Zeeman coeffcients $W_n^{(0)}$, $W_n^{(1)}$, and $W_n^{(2)}$, wave functions $|\phi\rangle$ at zero-field and calculated inverse susceptibilities χ^{-1} for: a) a free spin with $S=1$, b) for two spins $S_1=S_2=1/2$ coupled via isotropic AF exchange $J_{iso}<0$, c) for a $S=1$ exposed to uniaxial anisotropy $D'<0$ with the external magnetic field applied along the *z*-direction, and d) for a $S=1$ exposed to uniaxial anisotropy $D'<0$ with the external magnetic field applied along the *x*-direction.

(a) free $S=1$

State	$\|\phi\rangle$	$W_n^{(0)}$	$W_n^{(1)}$	$W_n^{(2)}$
$\|\phi\rangle_3$	$\|1,+1\rangle$	0	$+\mu_B g$	0
$\|\phi\rangle_2$	$\|1,0\rangle$	0	0	0
$\|\phi\rangle_1$	$\|1,-1\rangle$	0	$-\mu_B g$	0
	$\chi_{S_1}^{-1} = C_{S_1}^{-1} \cdot T$			(3)

(b) AF exchange between two $S=1/2$

State	$\|\phi\rangle$	$W_n^{(0)}$	$W_n^{(1)}$	$W_n^{(2)}$
$\|\phi\rangle_4$	$\|1,+1\rangle$	$-2J$	$+\mu_B g$	0
$\|\phi\rangle_3$	$\|1,0\rangle$	$-2J$	0	0
$\|\phi\rangle_2$	$\|1,-1\rangle$	$-2J$	$-\mu_B g$	0
$\|\phi\rangle_1$	$\|0\rangle$	0	0	0
	$\chi_{AF}^{-1} = C_{AF}^{-1} \cdot (T-\theta_{AF})$; $\theta_{AF}=J/2k_B$			(4)

(c) $D'<0$ (CF/ZFS) and field in *z*-direction

State	$\|\phi\rangle$	$W_n^{(0)}$	$W_n^{(1)}$	$W_n^{(2)}$
$\|\phi\rangle_3$	$\|1,0\rangle$	D'	0	0
$\|\phi\rangle_2$	$\|1,+1\rangle$	0	$+\mu_B g$	0
$\|\phi\rangle_1$	$\|1,-1\rangle$	0	$-\mu_B g$	0
	$\chi_{DZ}^{-1} = C_{DZ}^{-1} \cdot (T+\theta_{DZ})$; $\theta_{DZ}=D'/3k_B$			(5)

(d) $D'<0$ (CF/ZFS) and field in *x*-direction

State	$\|\phi\rangle$	$W_n^{(0)}$	$W_n^{(1)}$	$W_n^{(2)}$
$\|\phi\rangle_3$	$\|1,0\rangle$	D'	0	w_2
$\|\phi\rangle_2$	$-\frac{1}{\sqrt{2}}\|1,-1\rangle+\frac{1}{\sqrt{2}}\|1,1\rangle$	0	0	0
$\|\phi\rangle_1$	$-\frac{1}{\sqrt{2}}\|1,-1\rangle-\frac{1}{\sqrt{2}}\|1,1\rangle$	0	0	$-w_2$
	$\chi_{DX}^{-1} = C_{DX}^{-1}[2+\exp(D_T/T)]\ldots$ $\cdot[1-\exp(D_T/T)]^{-1}$; $D_T=D'/k_B$			(6)

The fit with χ_{DX}^{-1} returns a negative uniaxial ZFS parameter $D' = -140(1)\ \mathrm{cm}^{-1}$. However, the refined values from χ_{DX}^{-1} should not interpreted quantitatively, since χ_{DX}^{-1} has been derived by considering the application of a magnetic field perpendicular to the easy-axis of anisotropy, i.e. it actually only describes the susceptibility along a certain crystallographic axis, but the experimental susceptibility curve χ has been obtained for a polycrystalline sample with statistical orientation of the crystallites and orientations of the easy-axes. The statistical orientations of the crystallites is however difficult to integrate within the analytical mathematical approach via the Van Vleck equation and it is preferred therefore to solve this quantitatively by the computational approach presented in Section 2.2.2. The main purpose of the fit with χ_{DX}^{-1} here was to demonstrate by an

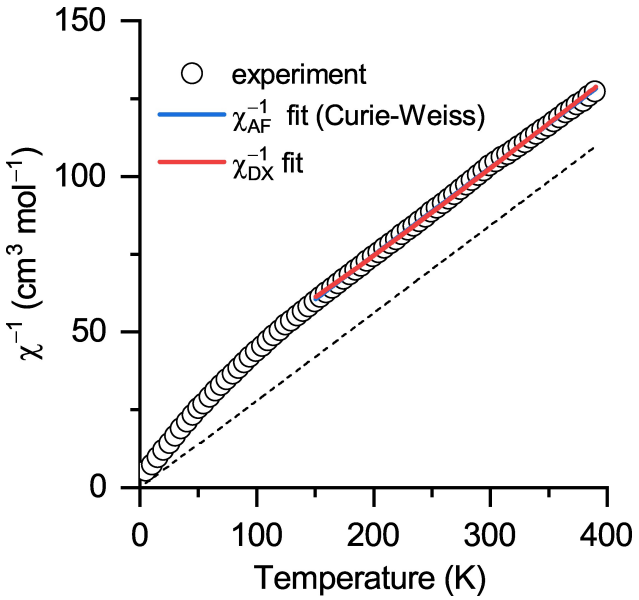

Figure 2. Experimentally obtained inverse molar susceptibility χ^{-1} vs. temperature for $Mg_3V_4(PO_4)_6$ (circles) and fits to the temperature region from 150 to 390 K by i) $\chi_{AF}^{-1} = C_{AF}^{-1}(T-\theta_{AF})$ (Curie-Weiss fit, see Eqs. (S4) to (S9) in SI) and by ii) $\chi_{DX}^{-1} = C_{DX}^{-1}[2+\exp(D_T/T)][1-\exp(D_T/T)]^{-1}$ (see Eqs. (S14) to (S16) in SI). The fits superimpose to high degree and the blue line can hardly be seen. The dashed line serves as guide for the eye. It exhibits the same slope as the fits but is shifted parallel to go through the origin.

analytical approach that the linear part of the χ^{-1} vs. temperature curve can not only be explained by AF exchange coupling but also by uniaxial single-ion anisotropy. It will turn out in the subsequent section that the D value as obtained by correctly implementing the statistics of a polycrystalline sample will approximately be 3 times that of D'.

2.2.2. Magnetic Model Refinement to DC Magnetometry Data

For simulating, interpreting and fitting of the DC magnetometry data, the PHI package[5] was used. By explicitly implementing the Zeeman term into the Hamiltonian, field-dependent magnetic properties can be calculated in a non-perturbative way in contrast to the approach via the Van Vleck equation. Further, the inclusion of orbital angular momentum beside spin orbital momentum allows for treating orbitally degenerate and strongly anisotropic ions by implementation of spin-orbit coupling and crystal field, respectively zero-field splitting effects. The Hilbert space for a system containing magnetic centers is built from the angular momentum basis states that are defined by every site's *i* total spin quantum number S_i and total orbital angular momentum number L_i. Since the Zeeman term is explicitly included in the Hamiltonian, the magnetic properties can be calculated from first principles without application of perturbation theory. A full mixing of all states by the magnetic field is considered and the magnetic properties are finally calculated via the relations $M \propto -\partial E/\partial B$ and $\chi \propto \partial M/\partial B$. Eq. (7) presents the phenomenological Hamiltonian whose individual terms (comprehensively described in Sec-

Research Article
doi.org/10.1002/ejic.202400162

tion S3.2 of the SI) refer to spin-orbit coupling (SO), exchange coupling (EX), crystal field (CF) interaction, zero-field splitting (ZFS), and to the Zeeman (ZEE) term:

$$\hat{H} = \hat{H}_{SO} + \hat{H}_{EX} + \left(\hat{H}_{CF} \vee \hat{H}_{ZFS}\right) + \hat{H}_{ZEE} \qquad \vee: \text{ or} \tag{7}$$

In this work, advantage is also taken of the isomorphism between an orbital triplet ground state T as associated with a ^3F term, for instance, and a triplet $L = 1$ from a P term ($M_L = 0, \pm 1$).[8] As an illustrative picture, the triplet T ground state can be thought to be represented by the occupation of the low lying t_{2g}-orbitals (in the one-electron picture) d_{xy}, d_{xz} and d_{zy} by the two electrons that pair to Spin $S = 1$, as it is the case for V^{3+} in octahedral crystal field, for instance. Within the framework of the so called *T-P*-isomorphism, these orbitals can then equivalently be described by the three p-orbitals p_x, p_y and p_z. These orbitals are three-fold degenerated in crystal field of cubic respectively octahedral ($m\bar{3}m$; O_h) point symmetry. A reduction from the octahedral to trigonal ($\bar{3}m$; D_{3d}) or tetragonal ($4/mmm$; D_{4h}) point symmetry lifts the three-fold degeneracy by moving p_z up in energy (representatively, such a lowering of point symmetry is also labelled as tetragonal in this work). In the picture of the *T-P*-Isomorphism, this is equivalent to a splitting of the T ground state into a double degenerated low lying E state and an excited non-degenerated A state and can be accounted for by introduction of the crystal field parameter (CFP) B_0^2 or the ZFS parameter D (the described situation holds for negative values of B_0^2 respectively D).[9] An additional reduction from trigonal respectively tetragonal point group symmetry to orthorhombic (mmm; D_{2h}), monoclinic ($2/m$; C_{2h}) or triclinic ($\bar{1}$; C_i) by a transverse crystal field further lifts the two-fold degeneracy of the p_x and p_y orbitals (representatively, such a lowering of point symmetry is also labelled as orthorhombic in this work). Or, in the picture of the isomorphism, this further splits the low lying two-fold degenerated E state (from T) into two non-degenerated A states. The additional reduction of point symmetry can be accounted for by the additional implementation of the transverse CFP B_2^2 (equivalent to the ZFS parameter E).[9] As outlined in detail in Ref. [10], there exits the isomorphism $\bar{T} \equiv \sigma' \bar{P}$ that connects the $\bar{L}$ matrix elements from an orbital triplet T state with those of an associated P state by the scalar $\sigma' = -A \cdot \kappa$. Within the framework of the *T-P*-Isomorphism, "A" takes the value 1 or 3/2 depending on whether it represents a T_2 or a T_1 orbital state, respectively. κ is the orbital reduction factor and accounts for reduction of the orbital momentum due to covalency or low symmetry effects and ranges between $0 < \kappa < 1$. As outlined in Section S3.2 of the SI, the orbital reduction parameter σ_r is connected to all orbital operators of the respective Hamiltonian terms. Therefore, within the used formalism of PHI, the *T-P*-isomorphism can be implemented by setting $\sigma_r = \sigma' = -A \cdot \kappa$ and by introducing an angular momentum $L_{TP} = 1$ that is connected to the spin S via the SO coupling constant λ_{TP}.

2.2.2.1. Model TP-ISO (T-P-Isomorphismus)

As supported by the SXAS analysis,[1] V can be considered to be present as V^{3+} in $Mg_3V_4(PO_4)_6$ with electronic configuration [Ar]$3d^2$ with total spin $S = 1$. As a free ion, the ground state is a $^3F_2$ term with a first excited $^3P_0$ term of equal spin that does however not play a role for magnetic properties, since its excitation is in the electron volt region. In an ideal octahedral crystal field, the $^3F_2$ term with seven-fold orbital multiplicity splits into a $^3T_1$ ground, a first excited $^3T_2$ and a second excited $^3A_2$ state. The $^3T_1$ ground state still possesses a partial orbital momentum that is however reduced considerably from $L = 3$ as present in the free ion. Further, the first excited $^3T_2$ state might further "mix" some orbital momentum into the ground state. To handle the crystal field splitting of the d-orbitals within the octahedral field, utilization of the *T-P*-Isomorphism is made with the starting assumption that V^{3+} is firstly coordinated by an ideal oxygen octahedron with O_h point symmetry. The magnetic model TP-ISO for a V^{3+} in a crystal field of ideal octahedral point symmetry is build up by a magnetic center represented by a spin quantum number $S = 1$, an orbital momentum quantum number $L_{TP} = 1$, a spin-orbit (SO) coupling constant λ_{TP} that couples the spin to the orbital momentum and an orbital reduction parameter $-\sigma_r = -A \cdot \kappa$, where $A = 3/2$ in the case of a T_1 ground state. The κ-parameter that accounts for a reduction of the orbital momentum due to covalency or low symmetry effects is initially set to 1 for the refinement, i.e. no reduction. Together, $\sigma_r = -3/2$ represents a d^2 in ideal octahedral coordination and is chosen as starting parameter for the refinement. Further, to account for a reduction of the octahedral point symmetry, the refinable CFP B_2^0 and B_2^2 are introduced that exclusively act on the orbital momentum (see Section S3.2). Figure 3a to c present the refinement of model TP-ISO to the χ, χ^{-1} and χT vs. temperature curves, respectively. Figure 3d presents the refinement of this model to the plots of magnetic moment M vs. field for 10 different temperatures ranging from 5 to 150 K. In total, the experimental DC magnetometry data can well be described by the TP-ISO magnetic model. All refined parameters are listed in Table 3b. The σ_r parameter has been refined to $-0.516(1)$, that is a very strong reduction of $-66\,\%$ compared to its starting value of $-3/2$. This points to a tremendous reduction of the orbital momentum contribution that can be explained by considerable deviations from the ideal octahedral coordination here. The considerable deviation from the ideal octahedral point symmetry removes the three-fold degeneracy of the triplet T_1 and quenches most of the orbital momentum. The results from the Curie-Weiss fit presented above already revealed that the contribution from orbital momentum is comparably small and that the observed paramagnetic moment is only 6% smaller compared to its spin-only moment. Simultaneously, the splitting of the triplet T_1 due to the symmetry lowering causes the single-ion anisotropy. This is also reflected by the refined high values of CFPs $B_0^2 = -200(3)\ \mathrm{cm}^{-1}$ and $B_2^2 = -237(2)\ \mathrm{cm}^{-1}$. The spin-orbit coupling parameter λ_{TP} has been refined to a value of 460(2) cm^{-1}.

Research Article
doi.org/10.1002/ejic.202400162

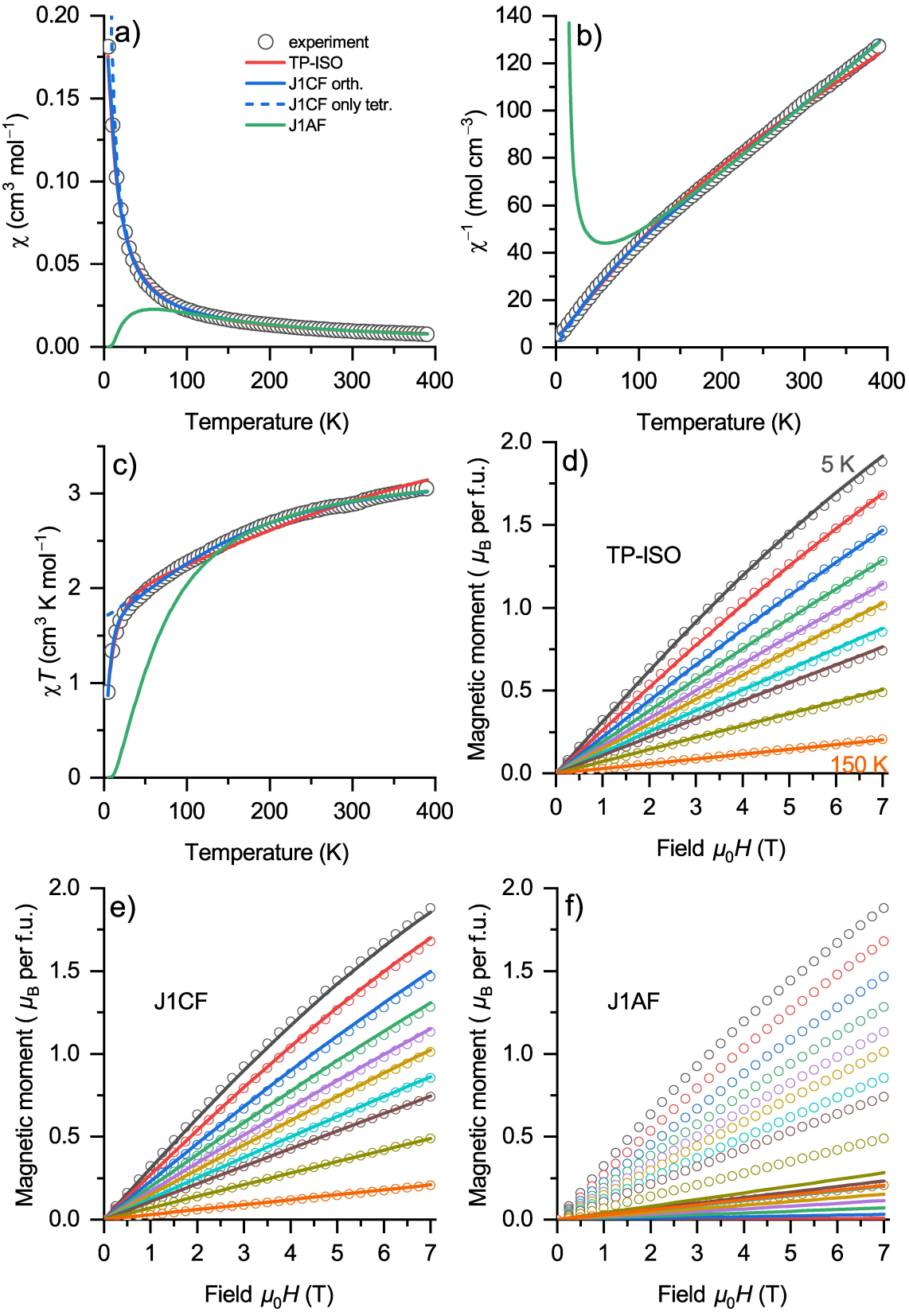

Figure 3. Experimentally measured DC magnetometry data for $Mg_3V_4(PO_4)_6$ (circles) fitted by the QM magnetic models TP-ISO, J1CF and J1AF models for a) susceptibility χ vs. T, b) inverse susceptibility χ^{-1} vs. T, and c) χT vs. T and the fits to the magnetization vs. field scans at various temperatures together with fits of the magnetic models d) TP-ISO, e) J1CF, and f) J1AF.

Research Article
doi.org/10.1002/ejic.202400162

Table 3. Results of fits to experimental DC magnetometry data: a) χ_{AF}^{-1} (Curie-Weiss) and χ_{DX}^{-1} fit to the inverse susceptibility χ^{-1} data from 150 to 390 K (Figure 2) and b) fit of the QM models TP-ISO, J1CF, J1AF, J1CFAF/Aniso and J1AF/Aniso to susceptibility data from 5 to 390 K (J1AF also for $T > 150$ K) as well as to magnetic field scans at various temperatures (Figure 3).

a) Van Vleck fit to χ^{-1} from 150 to 300 K		b) Spin Hamiltonian fit to complete $\chi(T)$ and $M(H,T)$ data from 5 to 390 K			
χ_{AF}^{-1}/Curie-Weiss (Figure 2)		TP-ISO (Figure 3)		J1AF (only > 150 K; Figure 3)	
see Eq. (4)		$S=1$ and $L_{TP}=1$		eff. angular mom. $J_{e1}=J_{e2}=1$	
C_{AF}	3.549(5) $cm^3\,K\,mol^{-1}$	σ_r	−0.516(1)	g_{iso}	1.836(8)
μ_{eff}	5.329(2) μ_B/f.u.	λ_{TP}	460(2) cm^{-1}	μ_{eff}	2.596(7) μ_B/V
μ_{eff}	2.663(2) μ_B/V	B_0^2	−200(3) cm^{-1}	J_{iso}	−20.26(9) cm^{-1}
θ_{AF}	−64.8(5) K	B_2^2	−237(2) cm^{-1}	$2J_{iso}/k_B$	−58.3(2) K
		Residual	$16\cdot10^{-4}$	Residual	$184\cdot10^{-4}$
χ_{DX}^{-1} (Figure 2)		J1CF (Figure 3)		J1AF (Figure S3)	
see Eq. (6)		eff. angular mom. $J_e=1$		eff. angular mom. $J_{e1}=J_{e2}=1$	
C_{DX}	0.050(1) $cm^{-3}\,mol$	g_{iso}	1.797(1)	g_{iso}	1.604(5)
D_T	−202(1) K	μ_{eff}	2.541(1) μ_B/V	μ_{eff}	2.27(1) μ_B/V
D'	−140(1) cm^{-1}	B_0^2 (= $D/3$)	−124(1) cm^{-1}	J_{iso}	−2.57(2) cm^{-1}
		$B_2^2 = E$	−6.80(1) cm^{-1}		
		Residual	$1.1\cdot10^{-4}$	fit not possible	
		J1CFAF/Aniso (Figure S5)		J1AF/Aniso (Figure S4)	
		eff. angular mom. $J_e=1$		eff. angular mom. $J_{e1}=J_{e2}=1$	
		g_{iso}	1.810(1)	g_{iso}	1.889
		μ_{eff}	2.560(1) μ_B/V	μ_{eff}	2.671 μ_B/V
		B_0^2/B_2^2	−129(1)/−6.00(1) cm^{-1}	J_z	+82.1 cm^{-1}
		$J_z/J_x = J_y$	−0.304(6)/−1.8(4) cm^{-1}	$J_x = J_y$	−84.7 cm^{-1}
		Residual	$0.5\cdot10^{-4}$	Residual	$2.1\cdot10^{-4}$

Due to the strong deviations from the octahedral symmetry with simultaneous considerable partial quenching of the orbital momentum contribution from the value that can be expected for the ideal octahedral symmetry with the T_1 ground term, the application of the TP-ISO model that "starts" with the highly symmetrical situation of an ideal octahedron appears inadequate. Especially, the circumstance that the transverse CFP B_2^2 has a larger absolute value than the axial CFP B_2^2 and the fact that both absolute value are quite high, give rise to set up a more appropriate model for the situation present for $Mg_3V_4(PO_4)_6$.

2.2.2.2. Model J1CF (Orthorhombic Crystal Field)

As revealed by the Curie-Weiss fit to the high temperature susceptibility data and also confirmed by the refined parameters of the TP-ISO model, the orbital momentum contribution to the total angular momentum is quite small and the effective paramagnetic moment for a V^{3+} is only slightly smaller than the spin-only value. Therefore, model J1CF follows the approach to ascribe an effective total orbital momentum J_e that is equal to the spin of the V^{3+} to describe a magnetic center, i.e. $J_e = S = 1$. Its total effective magnetic moment μ_{eff} is adjusted via an isotropic g_{iso}-factor to account for the orbital momentum contribution. In other words, the spin of a V^{3+} magnetic center is supposed to be only perturbed by the orbital momentum contributions. To account for the accompanied symmetry reductions and induced anisotropies due to the orbital momentum contribution, the effective total angular momentum $J_e = S = 1$ is exposed (as $L = J_e$) to a crystal field up to 2^{nd} order by introducing the CFP B_0^2 and B_2^2. Due to the equivalence of CFP up to second order and the ZFS formalism, also the refined ZFS parameters $D = 3B_0^2$ and $E = B_2^2$ will be listed accordingly. By introducing the CFPs up to second order, point symmetry reductions from octahedral (idealized coordination) to tetragonal or trigonal (by B_2^0) and further to orthorhombic, monoclinic or triclinic (by B_2^0 and B_2^2) can be accounted for as outlined above. As shown in Figure 3a–c and 3e, and listed in Table 3, model J1CF can explain the experimental data even slightly better than the model TP-ISO (see values of residuals).

The refined g_{iso} value of 1.797(1) corresponds to an effective magnetic moment of $\mu_{eff} = 2.541(1)\,\mu_B$/V in quite good agreement with the value deduced from the Curie constant that was extracted from the Curie-Weiss fit. Instead of isotropic also anisotropic $g_z = 1.814(1)$ and $g_x = g_y = 1.774(1)$ values can be refined with almost identical refined values for the CFPs. Normally, for refinements to magnetometry data, isotropic g-values are preferred in order to avoid over-parametrization. The CFPs were refined to $B_0^2 = D/3 = -124(1)\ cm^{-1}$ and

Research Article
doi.org/10.1002/ejic.202400162

$B_2^2 = E = -6.80(1)\ cm^{-1}$, respectively, revealing a point symmetry reduction from octahedral to orthorhombic or lower. Model J1CF is strongly related to the model that has already been applied in Ref. [1] with the very similar refined parameters $B_0^2 = D/3 = -119(1)\ cm^{-1}$ and $B_2^2 = E = -6.22(1)\ cm^{-1}$, respectively. The small differences compared to the value obtained here can be ascribed to a more profound correction of the raw data for diamagnetic contributions. Whereas in Ref. [1] only the contribution from the atomic closed shells has been considered, in this work also the diamagnetic contribution from the black carbon has explicitly be accounted for in a quantitative manner. The strong axial CFP B_0^2 rather affects the high temperature region of the susceptibility data. This is illustrated by the blue dashed line in Figure 3a–c that represents the modelled susceptibility if only B_0^2 would contribute (tetragonal anisotropy). The small transverse CFP B_2^2 is needed to correctly model the susceptibility progression at temperatures below approximately 50 K (orthorhombic anisotropy). Before a more comprehensive interpretation of these results will be given, it will shortly be outlined how these results can be related to the fit of χ_{DX}^{-1} to the susceptibility data from 150 to 390 K presented above that returned $D' = -140(1)\ cm^{-1}$, i.e. only about $D/3$. The reason is that χ_{DX}^{-1} only describes the situation for a selected single crystallographic direction perpendicular to the easy axis, but that actually the susceptibility measurement was obtained from a polycrystalline sample. If the refinement of model J1CF would be restricted to a temperature region from 150 to 390 K, only with axial anisotropy and with the field only applied in the *x*-direction (single crystal experiment instead of statistically averaging the field directions), then a parameter $D_{(x)} = -137(1)\ cm^{-1}$ would have been refined that is of similar magnitude as $D' = -140(1)\ cm^{-1}$.

The axial crystal field, parameterized by $B_0^2 < 0$ (tetragonal or trigonal point symmetry), causes the wavefunction $|\psi\rangle_3 = |1, 0\rangle_z$ to be uplifted in energy (ZFS), whereas the wavefunctions $|\psi\rangle_1 = |1, -1\rangle_z$ and $|\psi\rangle_2 = |1, +1\rangle_z$ remain at zero energy. As shown in the Zeeman diagram in Figure 4c, the energy difference between the ground state and the excited states is $W_3^{(0)} = 3|B_0^2| = |D| = 411(3)\ cm^{-1}$ at zero-field. The lower the temperature, the less $|\psi\rangle_3$ is thermally populated, and the higher is the population of the two low lying levels. As a consequence, with lowering the temperature the susceptibility within the *x*-*y*-plane is more and more reduced compared to that along the *z*-axis. For a magnetic field along the *z*-axis the ground state $|\psi\rangle_1$ exhibits the Zeeman coefficients $W_1^{(0)} = 0$, $W_1^{(1)} < 0$ and $W_1^{(2)} = 0$ and $|\psi\rangle_2$ the coefficients $W_2^{(0)} = 0$, $W_2^{(1)} > 0$ and $W_2^{(2)} = 0$ (Figure 4c).

When a magnetic field is set along the *x*- or the *y*-direction, it is advantageous, to choose another basis where the low lying $|\psi\rangle_1$ and $|\psi\rangle_2$ are equally intermixed with each other with different phases: $|\psi\rangle'_1 = 1/\sqrt{2}|1, -1\rangle_z + 1/\sqrt{2}|1, +1\rangle_z$, $|\psi\rangle'_2 = 1/\sqrt{2}|1, -1\rangle_z - 1/\sqrt{2}|1, +1\rangle_z = |1, 0\rangle_x$ and $|\psi\rangle'_3 = |1, 0\rangle_z$. By applying a field in *x*-direction (*y* would be equivalent), $|\psi\rangle'_2$ remains $|1, 0\rangle_x$ that is non-magnetic in this field direction. But the stronger the field in *x*-direction, the more $|\psi\rangle'_3 = |1, 0\rangle_z$ is mixed with a negative phase to $|\psi\rangle'_1$ resulting in more of $|1, -1\rangle_x = 1/2|1, -1\rangle_z + 1/\sqrt{2}|1, 0\rangle_z + 1/2|1, +1\rangle_z$ contribution to the lowest lying $|\psi\rangle'_1$ state. Simultaneously, more of the $|\psi\rangle'_1$ is mixed by the field with positive phase to $|\psi\rangle'_3 = |1, 0\rangle_z$, resulting in more of $|1, +1\rangle_x = 1/2|1, -1\rangle_z - 1/\sqrt{2}|1, 0\rangle_z + 1/2|1, +1\rangle_z$ contribution to the excited $|\psi\rangle'_3$ state. As a consequence, for fields in *x*-direction, the Zeeman coefficients of $|\psi\rangle'_1$ are $W_1^{(0)} = W_1^{(1)} = 0$ and $W_1^{(2)} < 0$, i.e. the Zeeman curve is slightly bent towards lower energies. To make this small effect visible the field axis in the Zeeman diagram shown in Figure 4d is strongly up scaled to 100 Tesla. The Zeeman coefficients of $|\psi\rangle'_2$ are $W_2^{(0)} = W_2^{(1)} = W_2^{(2)} = 0$, i.e. the Zeeman curve is a horizontal line. For the $|\psi\rangle'_3$ state that is lifted by $|D|$ at zero-field due to the uniaxial crystal field, the Zeeman coefficients are $W_3^{(0)} = |D|$, $W_3^{(1)} = 0$ and $W_3^{(2)} > 0$, i.e. the Zeeman curve is slightly bent towards higher energies. In Figure 4d the wavefunctions $|\psi\rangle_n$ at zero-field and $|\psi\rangle'_n$ at $H_{x,y}$ are both labelled as $|\psi\rangle_n$ for simplicity.

The role of the transverse axial field that has been refined to $B_2^2 = E = -6.23(1)\ cm^{-1}$ by application of model J1CF, is a little bit more subtle. A transverse crystal field is connected to a further symmetry reduction from tetragonal (or trigonal) to orthorhombic or lower point symmetry. Still within the framework of a *P* ($L = J_e = 1$) state that is represented by the effective total angular momentum $J_e = 1$ in model J1CF, the transverse crystal field in form of $B_2^2 = E$, removes the two-fold degeneracy of the ground state by lifting the $|\psi\rangle_2$ above the $|\psi\rangle_1$ state by an energy of $|E|$ in zero-field (see Figure 4e). The zero-field ground states are then modified to $|\psi\rangle'_1 = 1/\sqrt{2}|1, +1\rangle_z + 1/\sqrt{2}|1, -1\rangle_z$ and $|\psi\rangle'_2 = 1/\sqrt{2}|1, +1\rangle_z - 1/\sqrt{2}|1, -1\rangle_z$, each without a "permanent" magnetic moment as expectation value along the *z*-axis. By application of a field along the *z*-axis more of the $|1, -1\rangle_z$ is mixed into $|\psi\rangle'_1$ and more $|1, +1\rangle_z$ into $|\psi\rangle'_2$. That means, that a magnetic field along the *z*-axis firstly needs to create a certain magnetic moment along this direction "against" the transverse crystal field energy $|E|$.

For orthorhombic anisotropy, due to contributions from crystal field $B_0^2 = D/3 = -120(1)\ cm^{-1}$ and $B_2^2 = E = -6.23(1)\ cm^{-1}$ for fields along the *z*-direction (as shown in Figure 4e), the lowest state $|\psi\rangle'_1$ has the Zeeman coefficients $W_1^{(0)} = W_1^{(1)} = 0$ and $W_1^{(2)} < 0$, i.e. the Zeeman curve is slightly bent towards lower energies. $|\psi\rangle'_2$ is lifted by the energy $|E|$ above $|\psi\rangle'_1$ and has the Zeeman coefficients $W_2^{(0)} = |E|$, $W_2^{(1)} = 0$ and $W_2^{(2)} > 0$, i.e. the Zeeman curve is slightly bent towards higher energies. $|\psi\rangle'_3$ is lifted by the energy $|D| + |E|/2$ above $|\psi\rangle'_1$ and has the Zeeman coefficients $W_3^{(0)} = |D| + |E|/2$, $W_3^{(1)} = 0$ and $W_3^{(2)} = 0$, i.e. the Zeeman curve is horizontal. In Figure 4e the wavefunctions $|\psi\rangle_n$ at zero-field and $|\psi\rangle'_n$ at H_z are both labelled as $|\psi\rangle_n$ for simplicity.

The case of orthorhombic anisotropy and the field applied within the *x*- or *y*-direction (Figure 4f) will not be discussed explicitly. The situation is similar to the situation when the field is applied in *z*-direction as outlined previously, but with the difference that the absolute values of the second order Zeeman coefficients are even smaller compared with those for the *z*-direction $\left|W_{Hx}^{(2)}\right| \approx \left|W_{Hy}^{(2)}\right| < \left|W_{Hz}^{(2)}\right|$. In detail the sign of *E* determines whether the anisotropy along *x*- or along *y*-direction is stronger.

Research Article
doi.org/10.1002/ejic.202400162

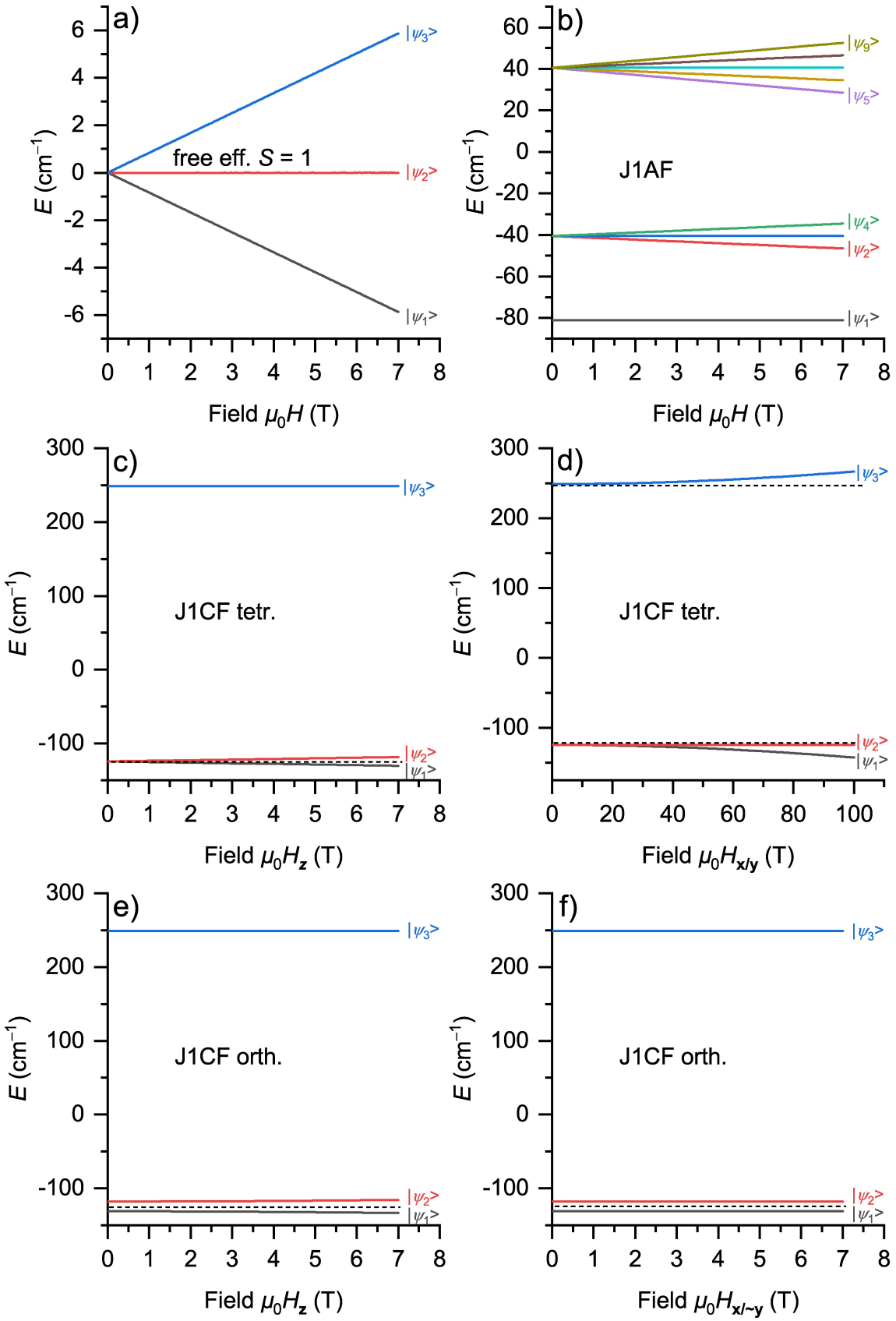

Figure 4. Simulated Zeeman diagrams using refined parameters of QM magnetic models obtained from fits to experimental data as shown in Figure 3. a) a free effective $J_e = 1$ with the g_{iso} values from model J1CF as a reference (B in *x*, *y*, or *z*-direction), b) model J1AF with parameters as obtained from the fit to χ from 150 to 390 K (*B* in *x*, *y*, or *z*-direction), c) for model J1CF in tetrahedral crystal field (*B* in *z*-direction), d) for model J1CF in tetrahedral crystal field (*B* in *x*- or *y*-direction), e) for model J1CF in orthorhombic crystal field (*B* in *z*-direction), and f) for model J1CF in orthorhombic crystal field (*B* in *x*-direction; in *y*-direction very similar).

Research Article
doi.org/10.1002/ejic.202400162

In summary, the DC magnetometry data obtained for $Mg_3V_4(PO_4)_6$ can well be described by model J1CF, that only considers single-ion anisotropy without any interactions between V ions. The refined crystal field parameters $B_0^2 = D/3$ cm^{-1} and $B_2^2 = E$ reveal a T_1 triplet splitting into three non-degenerated *A* terms due to a point symmetry reduction of the coordination polyhedron from octahedral O_h to orthorhombic, respectively monoclinic or triclinic. This point symmetry reduction, as indicated by the magnetic properties, is in agreement with the crystallographic structure details where V(1) and V(2) are located on 2*i* Wckoff sites with triclinic (1) point symmetry. However, as listed in Table 1 and highlighted in Figure 1 by green coloured bondings, the VO_6 units each exhibit one exceptionally short V(1)-O(2) respectively V(2)-O(10) distance compared to all other V–O distances. Therefore, the local coordination of V^{3+} is characterized by a strong uniaxial tetrahedral distortion in the first place, as reflected by the large absolute value of $|B_0^2|$, and further minor distortions that finally lead to a triclinic point symmetry, as reflected by the smaller $|B_2^2|$ value.

At temperatures above about 150 K, where the Curie-Weiss fits have been performed, the single-ion anisotropy can affect the evolution of the susceptibility with temperature in a very similar way as antiferromagnetic exchange coupling can do, as demonstrated in the previous section. The specific characteristics of single-ion anisotropy on the one side and magnetic exchange interactions on the other side, respectively their differences, get more pronounced at lower temperatures. In this context, it is also of importance that the magnetometry data have been obtained from a polycrystalline sample with a statistical distribution of crystallographic orientations of the individual crystallites. In this case, the statistical orientations of the crystallites implies a statistical distribution of the easy axes of anisotropy in all spatial directions. Application of a magnetic field that is comparably weak with respect to the anisotropy then causes the individual magnetic moments to point evenly distributed in all spatial directions of a hemisphere (as illustrated in Figure S2 in the SI). As outlined in detail in the SI Section S3.3, the total magnetic moment N_0 of a collection of free moments that would be obtained if they would be totally aligned, is reduced to half of their value $N_0/2$ if the same number of magnetic moments are forced to be distributed homogenously within such a hemisphere. That is, the easy-axis anisotropy, if realized to full extend, e.g. when it totally dominates over the Zeeman energy term at low temperature and moderate fields, decreases the magnetic moment respectively the susceptibility, but at maximum to half of the value compared to the free moments (for a polycrystalline sample!). This is a very specific and important difference compared to the case if there would exist an AF exchange interaction between the magnetic moments respectively the underlying spin angular moments instead (will be discussed below). An AF coupling reduces the magnetic net moment along the *z*-direction (direction of quantization and of applied magnetic field) more drastically at low temperature than the uniaxial single-ion anisotropy does (see also illustration in ToC figure). In a polycrystalline sample, uniaxial anisotropy only aligns the individual magnetic moments within a hemisphere and reduces the total magnetic moment along the *z*-direction to half of the value of hypothetical free moments, but AF coupling might cancel the net total magnetic moment along the *z*-direction completely at very low temperature. However, this picture is not complete yet, since so far only the uniaxial part of the single-ion anisotropy has been considered, i.e. the tetragonal anisotropy, without taking into account the additional contribution from the transverse crystal field, parameterized by $B_2^2 = E$ (orthorhombic anisotropy), that was shown to have a stronger effect for temperatures below approximately 50 K. In this very low temperature region, the transverse field kind of induces a tunneling of the magnetic moments along the easy-axis (via the orbital momenta) and thereby causes a cancelling of the expectation value of magnetization along the easy-axis. An applied magnetic field that contributes a Zeeman energy term then "competes" with the comparably small transverse crystal field and reinstalls again partially a magnetic moment parallel to the easy-axis direction. That means that the transverse crystal field $B_2^2 = E$ is capable to reduce the measured net magnetization more strongly at very low temperature than if only uniaxial anisotropy would be present.

2.2.2.3. Model J1AF (Antiferromagnetic Exchange Interaction)

In Section S3.1 we derived an expression from the Van Vleck equation for the susceptibility of two spins $S_1 = S_2 = 1/2$ centers that couple with each other AF via an isotropic exchange $J_{iso} < 0$ (see also Eqs. (S4) to (S9) in the SI). For two spins $S_1 = S_2 = 1/2$, there are three solutions with a total spin $S_{tot} = (S_1 + S_2) = 1$ (triplet) with an energy $E_{ex}^T = 1/2 \cdot J_{iso}$ and one solution with zero total spin (singulet) with an energy $E_{ex}^S = -3/2 \cdot J_{iso}$ (see also Table S3 in the SI). By restriction to AF coupling with $J_{iso} < 0$ the singulet state represents the ground state with the degenerated triplet states $2|J_{iso}|$ at higher energy in zero-field. The magnetic model J1AF as used for the phenomenological Hamiltonian approach should consist out of two spins $S_1 = S_2 = 1$ to more adequately reflect the situation of two AF coupling V^{3+} magnetic centers, each with spin $S = 1$. For two spins $S_1 = S_2 = 1$, the magnetic exchange coupling leads to one singulet ($S_{tot} = 0$) with energy $E_{ex}^S = -4J_{iso}$, a three-fold degenerated triplet ($S_{tot} = 1$) with energy $E_{ex}^T = -2J_{iso}$ and a five-fold degenerated pentalet ($P_{tot} = 2$) with energy $E_{ex}^S = +2J_{iso}$ (see also Table S3 in SI). In the case of AF exchange $J_{iso} < 0$, the singulet forms the ground state, with the triplet $2|J_{iso}|$ higher in energy and the pentalet $6|J_{iso}|$ above the ground state (see also Figure 4b). It is fact that the description of the low lying states is the same for $S_1 = S_2 = 1/2$ and $S_1 = S_2 = 1$ by separating the triplet by $2|J_{iso}|$ above the ground state singulet. The difference is that in the $S_1 = S_2 = 1$ case there is an additional pentalet state at high energy, but the magnetic properties will mainly be determined by the low lying singulet and triplet states. Therefore, the results of the Curie-Weiss fit that relies on the $S_1 = S_2 = 1/2$ case, describe the effect of AF exchange interaction on the magnetic susceptibility already quite well as verified below.

The model J1AF consists of two centers, each with an effective total angular momentum quantum number $J_e = S = 1$ representing a V^{3+} ion. An isotropic g_{iso}-factor that is constrained to the same value for both centers allows to refine an effective paramagnetic moment connected to the effective total angular momentum J_e. A refinement of model J1AF that is restricted to the temperature range from 150 to 390 K returns a refined effective magnetic moment of $\mu_{eff} = 2.596(7)\ \mu_B$/V in good agreement with the refined value of model J1CF and also with that obtained from the Curie-Weiss fit (see also Table 3). The isotropic exchange interaction constant is refined to $J_{iso} = -20.26(7)\ \mathrm{cm}^{-1}$ what corresponds to a an energy gap between the triplet and the singulet of $\Delta E_{T-S} = 2J_{iso}$ that is equal to $2J_{iso}/k_B = -58.3(2)$ K, expressed as thermal energy. This value is quite close to the Weiss constant $\theta_{AF} = -64.8(5)$ K as determined from the Curie-Weiss fit from 150 to 390 K in Section 2.2.1. The good agreement verifies the above mentioned assumption that the magnetic susceptibility is mainly determined by the low lying singulet and triplet state, since only these were considered for the derivation of the Curie-Weiss term (see Eqs. (S4) to (S9) of Section S3.1 in SI). However, when the refined parameters for μ_{eff} and J_{iso} as obtained from the fit from 150 to 390 K are used to simulate the complete temperature range and also the magnetization vs. field plots, there is a very strong deviation from the experimental curves. Whereas the high temperature region above about 150 K can adequately be described by the model J1AF, the extrapolated susceptibility values (green line in Figure 3a–c) at low temperatures are much too small (χ and χT) respectively much too high (χ^{-1}). Also the field scans (Figure 3f) are only correctly modelled for 150 K, but for the low temperatures the simulated values are much too low. An attempt to refine the model J1AF to the susceptibility data over the whole temperature range and to all field scans obtained for various temperatures was also not successful (see Table 3 and Figure S3 in SI).

2.2.2.4. Model J1AF/Aniso and J1CFAF/Aniso

QM model J1AF/Aniso is similar to model J1AF, but it allows for anisotropic AF exchange according to Eq. (S19) with $J_z \neq J_x = J_y$. A very good fit to the complete susceptibility vs. temperature and magnetization vs. field data sets was obtained as shown in Figure S4. The refined anisotropic exchange constants (see also Table 3) describe ferromagnetic exchange coupling in the *z*-direction $J_z = +82(1)\ \mathrm{cm}^{-1}$ and AF exchange coupling in the *x*- and *y*-direction with $J_x = J_y = -84(7)\ \mathrm{cm}^{-1}$. Anisotropic exchange parameters of that kind, with opposing sign for different directions, have also been reported for other compounds in literature. For instance, for a single-chain magnet built from an Os cyanidometallate(III) and a Mn(III) complex, anisotropic exchange parameters $J_x = -22$, $J_y = +28$, $J_x = -26\ \mathrm{cm}^{-1}$ have been published for the cyanide-bridged Os(III)-CN-Mn fragments.[11] These were compared with values of anisotropic exchange parameters for discrete trinuclear $Mn(III)_2Os(III)$ clusters with similar molecular structure $J_x = -18$, $J_y = +35$, $J_x = -33\ \mathrm{cm}^{-1}$,[12] respectively $J_x = -23.5$, $J_y = +32.0$, $J_x = -25.9\ \mathrm{cm}^{-1}$.[13] Anisotropic exchange parameters with opposing signs are therefore at least a known respectively reported phenomenon in principle. However, if both, single-ion anisotropy as realized in model J1CF and anisotropic AF exchange coupling as realized in model J1AF/Aniso, are both simultaneously introduced as refinable parameters in the QM magnetic model J1CFAF/Aniso, then a very good fit to the experimental data for the susceptibility and magnetic field scan data set can indeed be obtained as shown in Figure S5. But the exchange constants are then refined to very small values $J_z = -0.304(6)\ \mathrm{cm}^{-1}$ and $J_x = J_y = -1.8(4)\ \mathrm{cm}^{-1}$, whereas the CFP still play the absolute dominant role exhibiting similar values as those of the J1CF model (see Table 3). This result further supports that single-ion anisotropies play the absolute dominant role for $Mg_3V_4(PO_4)_6$ whereas exchange interactions can rather be neglected. As a consequence, in the authors' opinion, the refined anisotropic exchange parameters as obtained for the refinement of model J1AF/Aniso, with opposing signs, should not be interpreted as to represent real anisotropic AF exchange coupling, but are supposed to actually only mimic single-ion anisotropy. The strong postive J_z and simultaneously strong negative $J_x = J_y$ anisotropic exchange parameters simply lead to magnetic moments along the *z*-direction but suppress magnetic moments within the *x*-*y*-plane what is quasi identical with the mode of action of single-ion anisotropy.

From the crystal structure data it follows that the super exchange path V(2)-O(7)-V(2) creates an angle of $\angle = 104.5(2)^\circ$, and V(1)-O(12)-V(1) creates an angle of $\angle = 96.7(2)^\circ$. According to the Goodenough-Kanamori rules,[14–16] these angles close to 90° should favour either a ferromagnetic or a weak antiferromagnetic exchange interaction (strong AF are normally connected to angles close to 180°). Weak ferromagnetic exchange interactions between two V magnetic centers within a V_2O_{10} would not effectively modify what is determined already by the strong single-ion anisotropies and the acting of the Zeeman term that favours parallel alignment anyway. Since the easy-axes within the V_2O_{10} units exhibit a parallel orientation due to the inversion center that located in the middle of the connection line V(1)-V(1), respectively V(2)-V(2), a weak ferromagnetic interaction would not modify this situation effectively. On the other side, according to all results obtained in this work, AF exchange couplings between V magnetic centers, if present at all, can only play a negligible role compared to the single-ion anisotropy.

3. Conclusions

In conclusion, the magnetic properties of $Mg_3V_4(PO_4)_6$ are decisively determined by single-ion anisotropy and antiferromagnetic exchange coupling plays only a negligible role. The quite simple QM magnetic model J1CF is capable to describe the susceptibility temperature scan as well as the field scans over the whole temperature and field parameter space with good agreement. J1CF represents a single V^{3+} magnetic center by an effective total angular momentum J_e that is set equal to

Research Article
doi.org/10.1002/ejic.202400162

the total spin angular momentum of the d^2 ion: $J_e = S = 1$. Orbital momentum contribution is considered by an isotropic g-factor that has been refined to $g_{iso} = 1.797(1)$, corresponding to an effective paramagnetic moment of $\mu_{eff} = 2.541(1)\,\mu_B$, that is somewhat below the spin-only value 2.83 μ_B for a spin $S = 1$ due to spin-orbit coupling. The single-ion anisotropy is parameterized by the crystal field parameters $B_0^2 = -124(1)$ cm^{-1} and $B_2^2 = -6.80(1)$ cm^{-1}. The large absolute value of B_0^2 compared to that of B_2^2 points to the realization of a strong uniaxial anisotropy (tetragonal site symmetry) in the first place. The fact that $|B_2^2| \neq 0$ reveals a further reduction of the site symmetry to orthorhombic or lower. This is in agreement with the crystallographic structural data where the magnetic V^{3+} mainly occupies the sites V(1) and V(2) with nominal triclinic (1) point symmetry. The fact that a single V–O distance of the distorted VO_6 octahedra is exceptionally shorter than all other V–O distances is in agreement with the predominant uniaxial anisotropy as revealed by the magnetic properties. Many other V^{3+} ion containing systems have been reported, where single-ion anisotropy has been found to also play a decisive role.[17–21]

The experimental data cannot be explained by magnetic models that only consider isotropic antiferromagnetic exchange interactions between two V ions (J1AF). Models that include both, single-ion anisotropy and anisotropic exchange interactions (J1CFAF/Aniso) indeed can describe the experimental data, but the values of the anisotropic exchange interactions are then again refined to negligible small values, i.e. solely the single-ion anisotropy is capable again to model the data sufficiently. For that reason single-ion anisotropy is identified to determine the magnetic properties of $Mg_3V_4(PO_4)_6$ and not antiferromagnetic exchange interactions. What has already been speculated in Ref. [1], can be confirmed by the more elaborate and comprehensive evaluation of this work.

Further, it was demonstrated analytically, by application of the Van Vleck equation, that also single-ion anisotropy leads to a linear and origin shifted inverse susceptibility curve under certain conditions. As a consequence, a Curie-Weiss fit to the high temperature inverse susceptibility data might easily lead to the wrong perception that antiferromagnetic exchange interactions between V ions would determine the magnetic properties of $Mg_3V_4(PO_4)_6$. It is a wide spread approach in literature to interpret the Weiss constant θ_{CW} as indicative for the presence of magnetic exchange interactions, sometimes without further verification whether this is supported by the existence of a magnetic phase transition to an ordered state at low temperature. It would be desirable that this work contributes to take local anisotropy also into consideration as alternative explanation for non-zero Weiss constants, especially for those cases where no transition to an ordered state confirms what has been claimed based on a Curie-Weiss fit.

Methodological Section

The Supporting Information contains the theoretical and computational Section S3 and the experimental Section S4.

Supporting Information

The Supporting Information contains Table S1: Crystal structure data of $Mg_3V_4(PO_4)_6$, Table S2: Fit results of $\chi_{CW}^{-1} \propto (T - \theta_{CW})$ to the expression of susceptibility $\chi_{DX}^{-1} \propto [2 + \exp(D_T/T)][1 - \exp(D_T/T)]^{-1}$, Table S3: Wave functions and energies of AF coupling of $S_1 = S_2 = 1$ and $S_1 = S_2 = 1/2$, Table S4: Diamagnetic susceptibility χ_{CS} from the closed shell electrons for $Mg_3V_4(PO_4)_6$, Figure S1: AC susceptibility vs frequency scans at 1.8 K at various magnetic dc fields, Figure S2: Orientation of magnetic moments due to uniaxial single-ion anisotropy, Figure S3: Refinement of QM magnetic model J1AF to experimental magnetometry data, Figure S4: Refinement of QM magnetic model J1AF/Aniso to experimental magnetometry data, Figure S5: Refinement of QM magnetic model J1CFAF/Aniso to experimental magnetometry data, Figure S6: Raw data corrections for diamagnetic contributions, Figure S7: Simulated curves of χ_{DX}^{-1} vs. temperature, and Section S3.1: Calculation of susceptibilities from Van Vleck equation, Section S3.2: Angular momentum Hamiltonian for magnetic models, Section S3.3: Calculation of net z-component of magnetization, Section S4.1: Synthesis of $Mg_3V_4(PO_4)_6$, Section S4.2: Methods of Structural and chemical characterization, Section S4.3: Methods of DC magnetometry measurements and raw data corrections.

Acknowledgements

The authors acknowledge DESY (Hamburg, Germany), a member of the Helmholtz Association HGF, for the provision of experimental facilities. This research work has gained benefit from experiments that were carried out at PETRA III beamlines P02.1, P64, and P65 under the proposals I-20200558 and I-20190446. This work contributes to the research performed at CELEST (Center for Electrochemical Energy Storage Ulm-Karlsruhe) and was funded by the German Research Foundation (DFG) under Project ID 390874152 (EXC 2154: POLiS – Post Lithium Storage Cluster of Excellence). Open Access funding enabled and organized by Projekt DEAL.

Conflict of Interests

There are no conflicts of interest to declare.

Data Availability Statement

The data that support the findings of this study are available from the corresponding author upon reasonable request.

Keywords: single-ion anisotropy · exchange interaction · Curie-Weiss · magnetometry · Van Vleck

[1] Q. Fu, B. Schwarz, Z. Ding, A. Sarapulova, P. G. Weidler, A. Missyul, M. Etter, E. Welter, W. Hua, M. Knapp, S. Dsoke, H. Ehrenberg, *Adv. Sci. (Weinheim, Baden-Wurttemberg, Germany)* **2023**, *10*, e2207283.
[2] N. W. Ashcroft, N. D. Mermin, *Solid State Physics*, HRW international editions, Saunders College, *Fort Worth* **1988**.
[3] C. Kittel, *Einführung in die Festkörperphysik*, Oldenbourg, München, 13., korr. aufl. edition **2002**.
[4] S. H. Porter, J. Xiong, M. Avdeev, D. Merz, P. M. Woodward, Z. Huang, *Inorg. Chem.* **2016**, *55*, 5772.
[5] N. F. Chilton, R. P. Anderson, L. D. Turner, A. Soncini, K. S. Murray, *J. Comput. Chem.* **2013**, *34*, 1164.
[6] S. Boudin, A. Grandin, A. Leclaire, M. M. Borel, B. Raveau, *J. Solid State Chem.* **1995**, *115*, 140.
[7] H. Lueken, *Magnetochemie: Eine Einführung in Theorie und Anwendung*, Teubner Studienbücher Chemie, Vieweg + Teubner Verlag, Wiesbaden **1999**.
[8] M. E. Lines, *J. Chem. Phys.* **1971**, *55*, 2977.
[9] C. Görller-Walrand, K. Binnemans, Chapter 155 Rationalization of crystal-field parametrization, in *Handbook on the Physics and Chemistry of Rare Earths*, vol. 23, pages 121–283, Elsevier **1996**.
[10] F. Lloret, M. Julve, J. Cano, R. Ruiz-García, E. Pardo, *Inorg. Chim. Acta* **2008**, *361*, 3432.
[11] V. S. Mironov, E. V. Peresypkina, K. E. Vostrikova, *Molecules* **2023**, *28*.
[12] J. Dreiser, K. S. Pedersen, A. Schnegg, K. Holldack, J. Nehrkorn, M. Sigrist, P. Tregenna-Piggott, H. Mutka, H. Weihe, V. S. Mironov, J. Bendix, O. Waldmann, *Chemistry (Weinheim an der Bergstrasse, Germany)* **2013**, *19*, 3693.
[13] D. Pinkowicz, H. I. Southerland, C. Avendaño, A. Prosvirin, C. Sanders, W. Wernsdorfer, K. S. Pedersen, J. Dreiser, R. Clérac, J. Nehrkorn, G. G. Simeoni, A. Schnegg, K. Holldack, K. R. Dunbar, *J. Am. Chem. Soc.* **2015**, *137*, 14406.
[14] J. B. Goodenough, *Phys. Rev.* **1955**, *100*, 564.
[15] J. B. Goodenough, *J. Phys. Chem. Solids* **1958**, *6*, 287.
[16] J. Kanamori, *J. Phys. Chem. Solids* **1959**, *10*, 87.
[17] W. Rudziński, *J. Magn. Magn. Mater.* **2022**, *546*, 168687.
[18] B. Bechlars, D. M. D'Alessandro, D. M. Jenkins, A. T. Iavarone, S. D. Glover, C. P. Kubiak, J. R. Long, *Nat. Chem.* **2010**, *2*, 362.
[19] D. Papoutsakis, D. Grohol, D. G. Nocera, *J. Am. Chem. Soc.* **2002**, *124*, 2647.
[20] K. C. M. Westrup, F. S. Santana, D. L. Hughes, G. G. Nunes, J. F. Soares, A.-L. Barra, R. Sessoli, L. Sorace, *Appl. Magn. Reson.* **2020**, *51*, 1233.
[21] M. R. M. Saber, *Enhancing Magnetic Properties Of Molecular Magnetic Materials: The Role of Single-Ion Anisotropy*, Ph.D. thesis, Texas A&M University **2013**.

Manuscript received: March 21, 2024
Accepted manuscript online: April 19, 2024
Version of record online: May 28, 2024